Acta Chemica Scandinavica A 32 (1978) 209 – 217

Pyrite-like Phases in the Rh—Te System

ARNE KJEKSHUS,[a] TROND RAKKE[a] and ARNE F. ANDRESEN[b]

[a] Kjemisk Institutt, Universitetet i Oslo, Blindern, Oslo 3, Norway and [b] Institutt for Atomenergi, N-2007 Kjeller, Norway

The phase and structural relations in the Rh – Te system (from 66 to 74 atomic % Te; between 400 and 1100 °C) have been studied by X-ray and neutron diffraction, density, metallographic, and DTA measurements. $Rh_{1-t}Te_2$ (max. comp. range $0.00 \leqq t \leqq 0.20$) takes a pyrite type structure with disordered distribution of Rh atoms and vacancies. In the pyrite-like, Rh_3Se_8 type structure of Rh_3Te_8, Rh atoms and vacancies are ordered.

Rather fragmentary information is available on the Rh – Te system. Wöhler *et al.*[1] were apparently the first to make a distinct rhodium telluride, $RhTe_2$. Their synthesis was repeated by Biltz[2] who claimed that the composition was Rh_2Te_5 and suggested that the structure is of a pseudo FeS_2-*p* (*p* = pyrite) type. Later work by Geller[3] and Steen[4] could not confirm this suggestion. Geller[3] describes three phases: RhTe (NiAs type), $RhTe_2$, (FeS_2-*p* type), and $RhTe_2$ [$Cd(OH)_2$ type]. Non-stoichiometry of the FeS_2-*p* type phase is suggested by Steen.[4] However, the only phase properly characterized both with respect to composition and structure is Rh_3Te_2.[5]

With this background, a comprehensive examination of the entire Rh – Te system is required, and such a study is presently being carried out at this Institute. Since our original interest in this system concerned the FeS_2-*p* type phase, the research programme was initially designed to clarify the properties of this phase. The present report therefore focuses attention on phases occurring from 66 to 74 atomic % Te.

EXPERIMENTAL

The samples were prepared from 99.999 % Rh powder (Johnson, Matthey & Co.) and 99.999 % Te (Koch-Light Laboratories) by heating in evacuated, sealed silica capsules at fixed temperatures between 400 and 1200 °C (interrupted, when necessary, by crushings). Below 400 °C the reaction rates are extremely low, and no attempts have been made to obtain equilibrium conditions below this temperature. More details concerning temperature regulation and quenching experiments are described in Refs. 6 and 7.

All samples were examined microscopically and by powder X-ray (Guinier) diffraction [Cu$K\alpha_1$ radiation, KCl ($a = 6.2919$ Å) as internal standard] at room temperature (unit cell dimensions derived by applying the method of least squares). Most samples were also examined metallographically (etched with aqueous solutions of HNO_3 or HNO_3/HCl). The density of single phase samples (~ 2 g) was measured pycnometrically with kerosene as displacement liquid. The pycnometer was filled with kerosene under vacuum to remove gases adsorbed by the samples.

DTA and high temperature powder X-ray data were collected and treated as described in Ref. 7.

Room temperature powder neutron diffraction data were obtained using cylindrical sample holders of vanadium or aluminium and neutrons of wavelength 1.877 Å from the reactor JEEP II. The nuclear scattering lengths (in 10^{-12} cm) $b_{Rh} = 0.584$ and $b_{Te} = 0.580$ were taken from Ref. 8. In all cases, the least squares profile refinement programme of Rietveld[9] was applied in the final fitting of the variable parameters.

PHASE ANALYSIS

The Rh – Te system has proved to be rather complicated in the compositional range between 40 and 66 atomic % Te. Below 40 and above 74 atomic % Te the system appears, on the other hand, to be simple. However, our investigations in these compositional ranges are still in progress and the fol-

lowing comments on the phase relationships from 0 to 66 and from 74 to 100 atomic % Te are tentative.

(i). Comments on the Rh–Te system in the range 0 to 66 atomic % Te. The most metal-rich, intermediate phase in the Rh–Te system appears to be Rh_3Te_2.[5] This phase exists at temperatures above ~550 °C and exhibits no appreciable range of homogeneity. Below ~550 °C Rh_3Te_2 disproportionates into Rh (no solid solubility of Te in Rh could be detected) and a phase of approximate composition $RhTe_{0.9}$ (structure unknown). The latter does not appear to exist above ~550 °C where disproportionation into Rh_3Te_2 and an "NiAs-like" phase occurs. The NiAs type phase that Geller[3] reported to be of equi-atomic composition is, in fact, close to $RhTe_{1.1}$ [hexagonal; $a=3.987(1)$, $c=5.661(1)$ Å] with only a very narrow range of homogeneity. Below ~600 °C the NiAs type phase transforms to an "NiAs-like" phase with unknown superstructure.

In the compositional range from $RhTe_{1.1}$* to $RhTe_{1.9}$ there exists some 18 phases depending on composition, temperature, and various details concerning the preparational conditions. Some of these phases are, however, difficult to obtain (particularly in a pure state) since the reaction rates for their formation are low. The structures of these phases are, except for possibly four or five of them, probably intermediate between the NiAs and $Cd(OH)_2$ types with ordered or partially ordered distributions of Rh atoms and vacancies.

The $Cd(OH)_2$ type phase, $Rh_{1+u}Te_2$, covers a range of compositions at high temperatures. Fig. 1 shows the dependence of the room temperature (trigonal) unit cell dimensions (derived from quenched samples) on the compositional parameter u. The widest range of homogeneity, $0.225 \geqq u \geqq 0.055$ ($RhTe_{1.633}$ to $RhTe_{1.896}$), corresponds to the highest quenching temperature (1100 °C) used in these experiments. (Quenching experiments from above 1100 °C showed an unacceptable degree of irreproducibility.) High temperature X-ray diffraction fully confirms these results for the Te-rich side of $Rh_{1+u}Te_2$, but suggests that the homogeneity range is somewhat wider on the Rh-rich side than found by quenching. At 1100 °C this correction may shift the phase boundary to $u=0.30$ ($RhTe_{1.54}$). There is accordingly no indication of a continuous NiAs to $Cd(OH)_2$ type solid solution.

* Gross formulae or atomic % Te are used to denote nominal compositions.

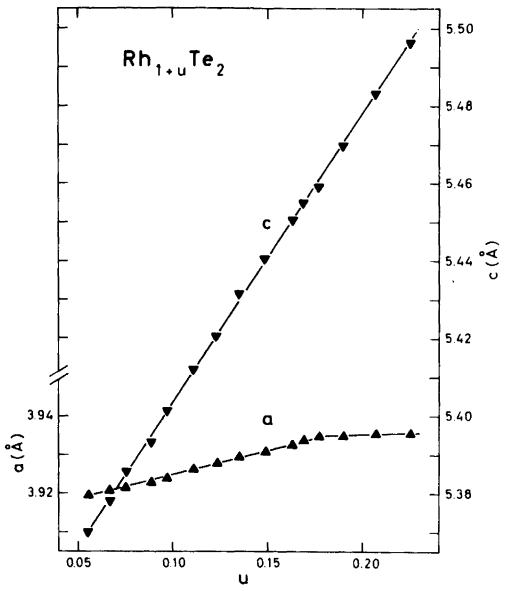

Fig. 1. Unit cell dimensions of (trigonal) $Rh_{1+u}Te_2$ as function of compositional parameter u. Samples quenched from 1100 °C. (Probable errors do not exceed size of symbols.)

The complication in determining the Rh-rich phase boundary below 1100 °C arises from the above-mentioned phases occurring between $RhTe_{1.1}$ and $RhTe_{1.9}$. The same complication renders the determination of the Te-rich phase boundary difficult below 550 °C.

(ii). The range 66 to 74 atomic % Te. Within the range 66 to 74 atomic % Te in the Rh–Te system there exist two intermediate phases (above 400 °C): a cubic (FeS_2-*p* type) phase, $Rh_{1-t}Te_2$, with Rh vacancies (*vide infra*) and a rhombohedrally deformed FeS_2-*p*-like phase, Rh_3Te_8 ($Rh_{0.75}Te_2$). Fig. 2 shows the room temperature unit cell edge and volume (the rhombohedral deformation, $\alpha=90.72°$, for Rh_3Te_8 is not shown) for quenched samples as a function of the compositional parameter t. From the numerous quenching experiments performed during this study, those samples shown to be pure according to X-ray diffraction, were further examined by metallographic methods and density measurements to ensure single phase preparations. The maximum compositional interval covered by the $Rh_{1-t}Te_2$ phase is $0.00 \leqq t \leqq 0.20$ as indicated in the upper part of Fig. 2. There is a distinct gap in composition between $Rh_{1-t}Te_2$ and Rh_3Te_8. The

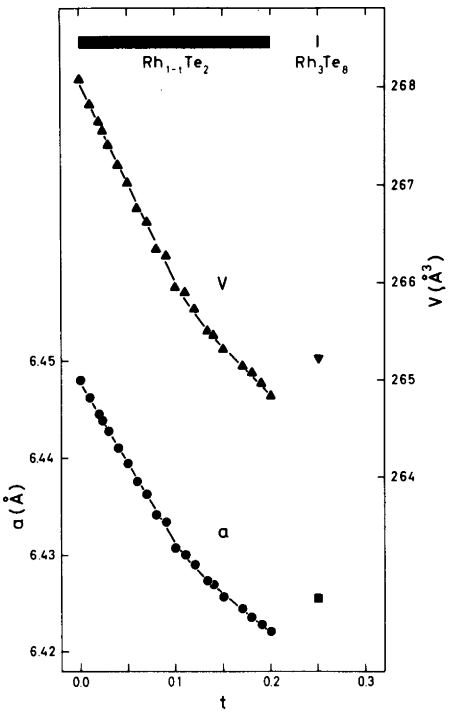

Fig. 2. Unit cell dimension and volume *versus* compositional parameter t for (cubic) $Rh_{1-t}Te_2$ (quenched samples). Data for Rh_3Te_8 are included for comparison. (Probable errors do not exceed size of symbols.)

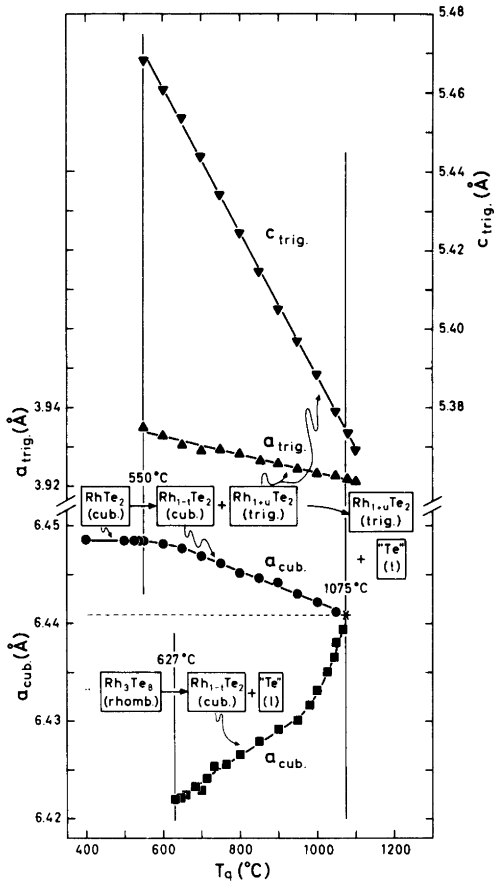

Fig. 3. Room temperature unit cell dimensions for samples of $RhTe_2$ and Rh_3Te_8 quenched from various temperatures T_q. (Probable errors do not exceed size of symbols.) Decomposition reactions are indicated and the notation "Te(l)" is conveniently used for a Te-rich (>95 atomic % Te; see text) liquid.

latter phase exhibits no appreciable range of homogeneity.

The homogeneity range of $Rh_{1-t}Te_2$ is sensitive to temperature, and below 550 °C the stoichiometric 1:2 composition is reached. The homogeneity range does not extend to lower Te contents than $RhTe_2$ at temperatures $\geqq$400 °C. The results of X-ray diffraction and metallographic examinations of quenched samples of $RhTe_2$ are summarized in Fig. 3. By combining the data in Figs. 2 and 3, the Rh-rich phase boundary of $Rh_{1-t}Te_2$ (Fig. 4) is obtained. Peritectic decomposition of $Rh_{1-t}Te_2$ ($t=0.040$) occurs at 1075±6 °C.

The presence of trigonal $Rh_{1+u}Te_2$ in $RhTe_2$ samples quenched from 550 °C is evident from metallographic examinations, whereas X-ray methods failed to detect the trigonal phase. For samples quenched from 600 °C, X-ray diffraction showed three lines. The unit cell dimensions for the trigonal phase at 550 and 600 °C in Fig. 3 therefore refer to measurements on more Rh-rich samples. The Te-rich boundary of the $Rh_{1+u}Te_2$ phase in Fig. 4 is determined by combining the data in Figs. 1 and 3.

In attempts to synthesize samples of nominal composition $RhTe_2$, reaction temperatures above 1075 °C produce the trigonal $Rh_{1+u}Te_2$ phase and liquid (Fig. 4). On cooling to 1075 °C, the peritectic composition, $Rh_{0.960}Te_2$, of the cubic phase and $Rh_{1.058}Te_2$ of the trigonal phase is first formed. At this temperature, equilibrium is established almost instantaneously. At lower (annealing) temperatures, equilibrium (stoichiometric $RhTe_2$ cannot be ob-

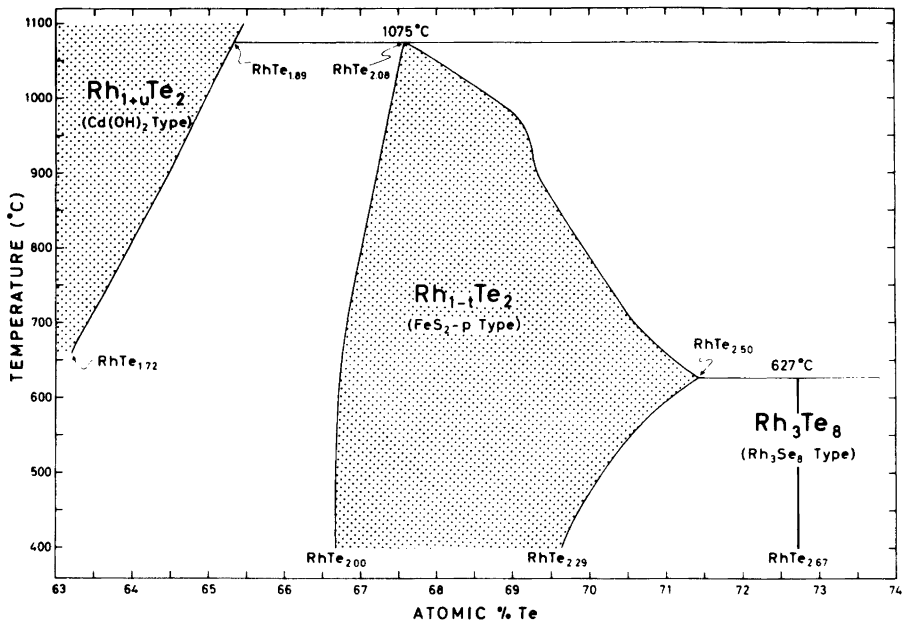

Fig. 4. Section of Rh – Te phase diagram.

tained above 550 °C; see above) is gradually attained more slowly, and even at 900 °C no change from the peritectic composition of the cubic phase could be detected within a few hours. Annealing for about a week at 900 °C is needed to establish true equilibrium conditions, which may explain how Geller[3] could find $a = 6.441(1)$ Å for the composition $RhTe_2$. This value for the cell edge matches, in reality, that for the peritectic composition, $Rh_{0.960}Te_2$.

Rh_3Te_8 decomposes peritectically at 627 ± 3 °C, explaining why Geller[3] and Steen[4] missed this phase by applying too high reaction and annealing temperatures. The quenching experiments on Rh_3Te_8 (Fig. 3) also serve to determine the Te-rich phase boundary of $Rh_{1-t}Te_2$ above 627 °C. At the peritectic temperature, the most Te-rich composition of $Rh_{1-t}Te_2$ ($t = 0.200$) is found.

The Te-rich phase boundary of $Rh_{1-t}Te_2$ below 627 °C is determined from a separate set of quenched samples, making, *inter alia*, use of the relation between unit cell dimension and composition shown in Fig. 2. On gradually turning to lower temperatures, these experiments become more and more time-consuming due to the long annealing periods required to obtain equilibrium. Below 400 °C overall annealing periods of up to two years were insufficient to achieve equilibrium conditions.

(iii). Comments on the Rh – Te system in the range 74 to 100 atomic % Te. At temperatures above 400 °C, no intermediate phase appears to exist between 74 and 100 atomic % Te. Over the compositional range 74 to 90 atomic % Te, DTA peaks at 450, 627, and 1075 °C could be interpreted as eutectic, peritectic, and peritectic temperatures, respectively. At still higher Te contents, the DTA curves were featureless except for the 450 °C peak. Metallographic examination of quenched samples has not yet been fully accounted for, but it seems that the liquidus reaches 1100 °C at 95 atomic % Te. The liquidus is probably lowered to 950 °C at 97 atomic % Te, and the eutectic composition must be located very near to 100 atomic % Te. (No solid solubility of Rh in Te could be detected.)

STRUCTURES

(i). Structure of the $Rh_{1-t}Te_2$ phase. The $Rh_{1-t}Te_2$ phase exhibits cubic symmetry and density (ranging between 8.84 g/cm^3 for $RhTe_2$ and 8.43 g/cm^3 for $Rh_{0.800}Te_2$); measurements show four $Rh_{1-t}Te_2$ formula units per unit cell. The systematic extinctions in the X-ray and neutron powder diffraction patterns (12 to 15 observed reflections) strongly suggest an overall FeS_2-*p* type atomic arrangement.

Table 1. Structural data for selected compositions of the $Rh_{1-t}Te_2$ phase.

	$RhTe_2$	$Rh_{0.980}Te_2$	$Rh_{0.950}Te_2$	$Rh_{0.931}Te_2$	$Rh_{0.900}Te_2$	$Rh_{0.862}Te_2$	$Rh_{0.820}Te_2$
a (Å)	6.4481(7)	6.4442(6)	6.4394(7)	6.4363(8)	6.4307(8)	6.4272(9)	6.4234(9)
x	0.3671(5)	0.3681(4)	0.3697(4)	0.3699(5)	0.3697(5)	0.3700(4)	0.3701(5)

At temperatures $\geqq 400$ °C, no superstructure reflections originating from an ordering of Rh atoms and vacancies (denoted □ in the formulae) could be detected for $t \neq 0$. (The possibility of ordered structures at temperatures below 400 °C is, on the other hand, open for further investigation.) According to space group $Pa3$ appropriate to the FeS_2-p type structure assumed for $Rh_{1-t}\square_tTe_2$, Rh atoms and vacancies are statistically distributed in position 4(*a*), and Te in 8(*c*).

Seven different samples: $RhTe_2$, $Rh_{0.980}Te_2$, $Rh_{0.950}Te_2$, $Rh_{0.931}Te_2$, $Rh_{0.900}Te_2$, $Rh_{0.862}Te_2$, and $Rh_{0.820}Te_2$ were subjected to structural refinements by the powder neutron diffraction/profile refinement technique. The assumption of FeS_2-p type structure for $Rh_{1-t}\square_tTe_2$ was confirmed by the rather low values of 0.019 to 0.034 obtained for the final neutron diffraction reliability factors. The defect concentrations (t) were also verified by varying the occupation numbers in preliminary refinement cycles.

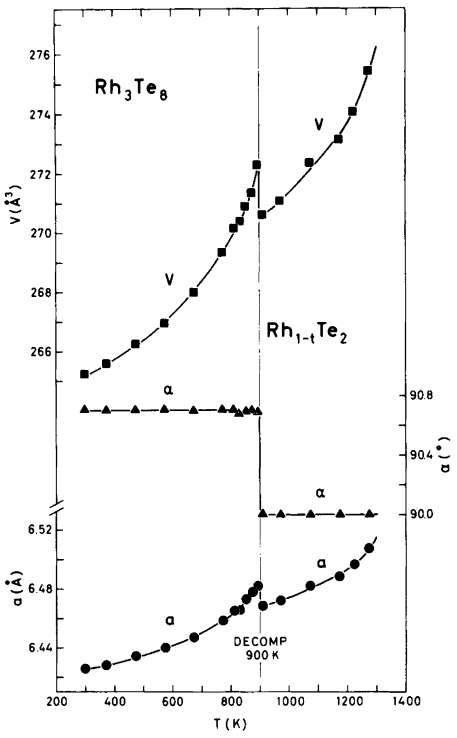

Fig. 5. Unit cell dimensions of (rhombohedral) Rh_3Te_8 *versus* temperature. For $T \geqq 900$ K: $Rh_3Te_8 \rightarrow Rh_{1-t}Te_2$ with variable t. (Probable errors do not exceed size of symbols.)

The room temperature (22 °C) values of the unit cell edge (a) and the positional parameter (x) for Te are listed in Table 1. The data show that the size of the unit cell decreases steadily (see also Fig. 2) with increasing number of vacancies, whereas x increases in the sequence $RhTe_2$, $Rh_{0.980}Te_2$, $Rh_{0.950}Te_2$, and remains approximately constant for higher values of t. The derived interatomic distances and angles are discussed in section *iii*.

(ii). Structure of the Rh_3Te_8 phase. The compound Rh_3Te_8 exhibits rhombohedral symmetry, and density (8.30 g/cm^3) measurements confirm one Rh_3Te_8 formula unit per unit cell. The additional reflections superimposed on the FeS_2-p type diffraction pattern, suggest an ordered, rhombohedrally distorted FeS_2-p type variant, $Rh_{0.75}\square_{0.25}Te_2$, isostructural with Rh_3Se_8.[10] As judged from high temperature X-ray diagrams, not even a partial disordering of the Rh atoms and vacancies occurs above room temperature. Fig. 5 shows the unit cell dimensions of Rh_3Te_8 as function of temperature, the apparent transition to cubic symmetry at 900 K being in reality a peritectic decomposition according to $Rh_{0.75}Te_2 \rightarrow Rh_{0.80}Te_2 + \text{liq}$.

As pointed out in Ref. 10, the only possible rhombohedral space groups permitting an atomic arrangement similar to the FeS_2-p type are $R3$ and $R\bar{3}$. Choosing $R\bar{3}$, places Rh in position 3(*e*) and the two crystallographically non-equivalent Te_I and Te_{II} atoms in 2(*c*) and 6(*f*), respectively.

The room temperature unit cell dimensions (a,α), the positional parameters (x_I, x_{II}, y_{II}, z_{II}) for Te_I and Te_{II}, and interatomic distances and angles are listed in Table 2. The rather low value of 0.038 for the final neutron diffraction reliability factor (based on profile refinement of 28 observed reflections) shows

Table 2. Structural data for the Rh_3Te_8 phase.

a (Å)		6.4255(4)	$Rh-Te_I$(Å)	×2 2.668(8)
α (°)		90.724(7)	$Rh-Te_{II}$(Å)	×2 2.653(6)
x_I		0.3683(12)	$Rh-Te_{II}$(Å)	×2 2.704(6)
x_{II}		0.8823(9)	□ $-Te_{II}$(Å)	×6 2.615(6)
y_{II}		0.1279(9)	Te_I-Te_I(Å)	×1 2.894(22)
z_{II}		0.6326(9)	$Te_{II}-Te_{II}$(Å)	×1 2.820(16)
$Te_I-Rh-Te_{II}$(°)	×2	86.2(2)	$Rh-Te_I-Rh$ (°)	×3 118.0(3)
$Te_I-Rh-Te_{II}$(°)	×2	93.8(2)	$Rh-Te_I-Te_I$(°)	×3 98.3(3)
$Te_I-Rh-Te_{II}$(°)	×2	82.8(2)	$Rh-Te_{II}-Rh$(°)	×1 114.9(2)
$Te_I-Rh-Te_{II}$(°)	×2	97.2(2)	□ $-Te_{II}-Rh$(°)	×1 116.1(2)
$Te_{II}-Rh-Te_{II}$(°)	×3	86.4(2)	□ $-Te_{II}-Rh$ (°)	×1 120.4(2)
$Te_{II}-Rh-Te_{II}$(°)	×2	93.6(2)	$Rh-Te_{II}-Te_{II}$(°)	×1 97.7(2)
$Te_{II}-$□$-Te_{II}$ (°)	×6	82.8(2)	$Rh-Te_{II}-Te_{II}$(°)	×1 100.0(2)
$Te_{II}-$□$-Te_{II}$ (°)	×6	97.2(2)	□ $-Te_{II}-Te_{II}$ (°)	×1 101.7(2)

that the assignment of an Rh_3Se_8 type structure to Rh_3Te_8 must be essentially correct.

(iii). Comparison between the $Rh_{1-t}Te_2$ and Rh_3Te_8 structures. Starting from $RhTe_2$ and its regular FeS_2-*p* type structure, the coordination polyhedron around Rh is that of a slightly distorted $Rh-Te_6$ octahedron (equal Rh – Te distances, Te – Rh – Te angles about 6° different from 90°). The immediate surroundings of Te amount to a distorted $Te-TeRh_3$ tetrahedron (with Te – Rh and Te – Te distances of different length and correspondingly different Rh – Te – Rh and Rh – Te – Te

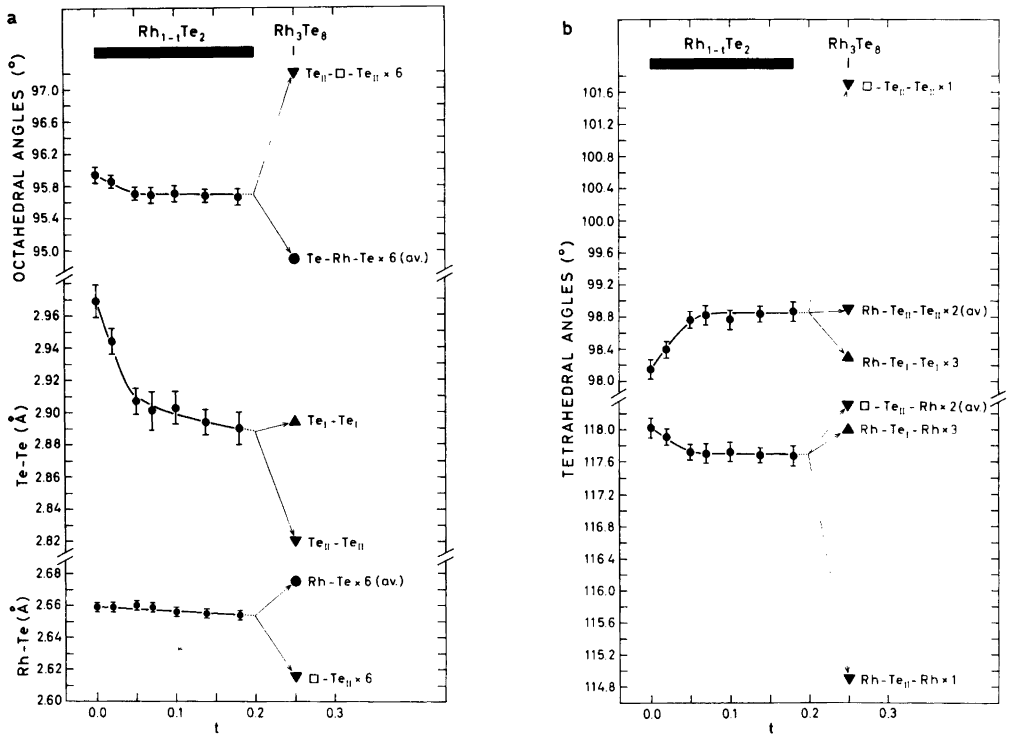

Fig. 6. Variation of bond lengths and bond angles for $Rh_{1-t}Te_2$ with t and in relation to Rh_3Te_8.

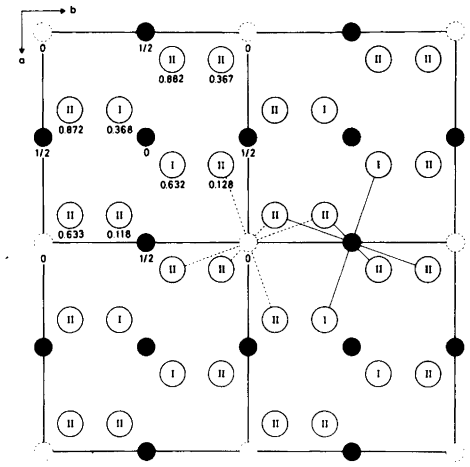

Fig. 7. Four unit cells of the Rh_3Te_8 structure projected along $[00\bar{1}]$, neglecting the rhombohedral distortion. Rh and Te atoms are indicated by filled and open circles, respectively, Rh vacancies by broken circles. (Fractions give z coordinates.)

angles). On turning to the metal deficient $Rh_{1-t}\square_tTe_2$ phase, the Rh–Te (□–Te) and Te–Te bonding interatomic distances, octahedral and tetrahedral bonding interatomic angles vary with t as shown in Fig. 6.

The perhaps most interesting feature emerging from Fig. 6 concerns the Te–Te distance and its functional dependence on t. For $RhTe_2$ this distance amounts to 2.97 Å, which must be considered as a rather long bonding Te–Te distance. For increasing t in $Rh_{1-t}\square_tTe_2$, the Te–Te distance decreases gradually towards the more common value 2.89 Å. Less marked are the overall decrease in the Rh–Te distance and the variations in the independent bond angles.

The kind of ordering of Rh and vacancies in Rh_3Te_8 is illustrated in Fig. 7, where the rhombohedral distortion from an FeS_2-*p* type arrangement is neglected in the plane of projection. An idealized version of the Rh_3Te_8 structure can be described in terms of only one variable parameter (x_0) as follows: $x_I = x_0$, $x_{II} = 1/2 + x_0$, $y_{II} = 1/2 - x_0$, and $z_{II} = 1 - x_0$. Extrapolation of the trend for $Rh_{1-t}Te_2$ (Table 1) gives for a hypothetical, disordered $Rh_{0.75}Te_2$, $x_0 = 0.370$ which may also represent a reasonable value in the idealized Rh_3Te_8 structure. The actual Rh_3Te_8 atomic arrangement is obtained from the idealized structure by further displacement of the atoms, *inter alia*, to make the Rh–Te_6 and □–Te_6 octahedra different (Fig. 6). Another, probably important difference concerns the Te–Te bond lengths: 2.89 Å for Te_I–Te_I *versus* 2.82 Å for Te_{II}–Te_{II}. (This distinction in bond lengths is not reported[10] for the corresponding Se_I–Se_I and Se_{II}–Se_{II} bonds in the isostructural Rh_3Se_8. To proceed further in the understanding of the rhodium tellurides, the latter result should be verified, and a redetermination of the Rh_3Se_8 structure is now being carried out by the present authors.)

The coordination polyhedron around Rh in Rh_3Te_8 is a distorted octahedron (Table 2). The three independent Rh–Te distances and the corresponding Te–Rh–Te angles are averaged in Fig. 6. The immediate surroundings of the vacancy are, on the other hand, similar to the octahedral arrangement in the FeS_2-*p* type structure. Te_I is surrounded by a Te_IRh_3 tetrahedron similar to that in stoichiometric $RhTe_2$, whereas Te_{II} "sees" one Te_{II}, two Rh, and a vacancy in a distorted tetrahedral arrangement (Table 2 and Fig. 6).

CORRESPONDING PHASES IN RELATED SYSTEMS

Unexpectedly Rh_3Te_8 decomposes peritectically rather than undergoing transformation to the disordered state characteristic of the $Rh_{1-t}Te_2$ phase. The reason for this behaviour is not understood and complementary data for related systems would be most helpful. In common with the rhodium tellurides, most of these systems have, however, only been fragmentarily studied. To remedy this situation, systematic studies on other systems have been started at this Institute. Here we shall briefly consider phases occurring between 66 and 74 atomic % X (X = S, Se, Te) on the basis of our preliminary results and literature data.

A separate $Rh_{1-t}S_2$ phase appears not to exist in the Rh–S system (*cf.* Ref. 11), whereas we can unequivocally confirm the occurrence of a rhombohedrally distorted phase. This phase has a composition very close to Rh_3S_8, $a = 5.5910(17)$ Å, but an unexpectedly small rhombohedral distortion, $\alpha = 90.19(3)°$. Further investigations are needed to determine its structure and to establish whether or not rhomohedral Rh_3S_8 transforms into a cubic (disordered) phase at higher temperatures.

The system Rh–Se appears to be more similar to the Rh–Te system in that the cubic phase, $Rh_{1-t}Se_2$, and the rhombohedral, Rh_3Se_8 [a=

5.9632(4) Å, $\alpha = 90.774(8)°$], both exist. However, close to the composition $RhSe_2$ an additional phase,[12] isostructural with $IrSe_2$,[13] occurs, and the location and temperature dependence of the homogeneity range of $Rh_{1-t}Se_2$ is reported[12] to differ substantially from that of $Rh_{1-t}Te_2$. According to our results, the difference is far less than earlier assumed, and mainly concerns the fact that the composition $RhSe_2$ is never reached for the $Rh_{1-t}Se_2$ phase. Apart from this, the shape of the Rh-rich phase boundary of $Rh_{1-t}Se_2$ appears to be similar to that for $Rh_{1-t}Te_2$ (Fig. 4).

The Se-rich phase boundary of $Rh_{1-t}Se_2$ is reported[12] to extend to $t \approx 0.25$ at temperatures between 800 and 900 °C, where the decomposition of Rh_3Se_8 is also assumed.[12] Hence, a phase transition between the rhombohedral and a cubic structure is possible. We have not, however, found any indications that this is the case, and although $Rh_{1-t}Se_2$ extends to larger t values than $Rh_{1-t}Te_2$, there is a distinct gap in composition between $Rh_{1-t}Se_2$ and Rh_3Se_8. Rh_3Se_8 disappears at ~855 °C (according to quenching experiments and high temperature X-ray data, but not detectable by DTA), where a peritectic reaction gives the cubic $Rh_{1-t}Se_2$ phase ($t \sim 0.23$).

Apart from Munson's[14] preparation of FeS_2-*p* type IrS_2 by high pressure–high temperature methods, cubic $Ir_{1-t}S_2$ or $Ir_{1-t}Se_2$ phases have not been synthesized in the Ir–S or Ir–Se systems by more conventional methods. However, phases with approximate compositions IrS_2 and $IrSe_2$ do exist[15] (*cf.* also Ref. 11), but these exhibit the $IrSe_2$ type structure[13] rather than the FeS_2-*p* type. Phases with compositions Ir_3S_8 and Ir_3Se_8 and with FeS_2-*p*-like structures are, on the other hand, registered in these systems.[10,11,15,16] The actual structures and transformation properties of these phases are hitherto unpublished. Our findings indicate that the formula Ir_3S_8 is very nearly correct and that the structure of this phase is of the Rh_3S_8 type. The situation is more complicated in the Ir–Se system, where two distinct FeS_2-*p*-like phases appear to exist with composition around Ir_3Se_8. One of these phases is probably of the Rh_3S_8 type.

Two phases $IrTe_2$ and Ir_3Te_8 have previously been found[17] in the Ir–Te system. $IrTe_2$ exhibits the $Cd(OH)_2$ type structure which is presently confirmed [trigonal; $a = 3.9297(8)$, $c = 5.3958(15)$ Å] to be of the stoichiometric 1:2 composition without any appreciable range of homogeneity [thus contrasting the $Cd(OH)_2$ type phase in the Rh–Te system]. At temperatures below ~650 °C, a new phase (not detected by Hockings and White[17]) is stabilized. This phase, of yet unknown structure, appears to be a proper low temperature modification in that it attains the same stoichiometric 1:2 composition. Transformations between the two modifications of $IrTe_2$ are slow and are not detectable by DTA methods. Ir_3Te_8 is reported[17] to take the FeS_2-*p* type structure, *viz.* $Ir_{0.75}\square_{0.25}Te_2$ with Ir atoms and vacancies statistically distributed. This phase has presently been confirmed, $a = 6.4138(6)$ Å, but we have not yet refined the structure, nor determined the exact composition (between $IrTe_{2.67}$ and $IrTe_{2.72}$). No appreciable range of homogeneity as a function of temperature (between 650 and 920 °C) could be found for this phase, thus contrasting $Rh_{1-t}Te_2$ both in this respect and also with regard to the number of vacancies which may be accommodated in the metal sublattice.

The disordered, FeS_2-*p* type Ir_3Te_8 phase transforms at lower temperatures to either another cubic phase (distinctly different from the disordered FeS_2-*p* type structure), $a = 6.4177(9)$ Å, or to a rhombohedral phase, $a = 6.4183(8)$ Å and $\alpha = 90.47(2)°$, depending on the preparational conditions (particularly the thermal history of the sample). High temperature X-ray studies of both these "low temperature" phases suggest that they transform continuously to the disordered FeS_2-*p* type at 650 °C (undetectable by DTA). The reverse reactions are very slow and reaction periods of the order of a year may be indicated, thus explaining why Hockings and White[17] did not detect these phases. A DTA signal at 920 °C could be interpreted as the peritectic $Ir_{0.75}Te_2 \rightarrow IrTe_2 + \text{liq.}$ decomposition.

The low temperature rhombohedral (probably isostructural with Rh_3Te_8) and cubic (or nearly cubic; allowing for uncertainty due to somewhat diffuse X-ray reflections) phases of Ir_3Te_8 appear to be essentially of the same type with respect to ordering of Rh atoms and vacancies. Thus, it seems possible to obtain an ordered structure with no (or very small) rhombohedral distortion.

On concluding the present survey on these phases, it appears appropriate to emphasize that the FeS_2-*p*-like phases in the Rh–S, Ir–S, Ir–Se, and Ir–Te systems are markedly similar with respect to the existence of only 3:8 compounds, which may transform from ordered to disordered structures. The Rh–Se and Rh–Te systems differ from the

others by taking two compositionally different FeS_2-*p*-like phases of which $Rh_{1-t}Se_2$ and $Rh_{1-t}Te_2$ exhibit broad ranges of homogeneity. Although Rh_3Se_8 and Rh_3Te_8 have well-defined stoichiometric compositions, they differ from their homologues in the degree of rhombohedral deformation and also by undergoing peritectic decompositions rather than order-disorder transformations at higher temperatures.

REFERENCES

1. Wöhler, L., Ewald, K. and Krall, H. G. *Ber. Dtsch. Chem. Ges. 66* (1933) 1638.
2. Biltz, W. *Z. Anorg. Allg. Chem. 233* (1937) 282.
3. Geller, S. *J. Am. Chem. Soc. 77* (1955) 2641.
4. Steen, Ø. *Thesis*, University of Oslo, Oslo 1955.
5. Zachariasen, W. H. *Acta Crystallogr. 20* (1966) 334.
6. Kjekshus, A. and Rakke, T. *Acta Chem. Scand. A 29* (1975) 443.
7. Kjekshus, A. and Rakke, T. *Acta Chem. Scand. A 31* (1977) 517.
8. *The 1977-Compilation of the Neutron Diffraction Commission.*
9. Rietveld, H. M. *J. Appl. Crystallogr. 2* (1969) 65.
10. Hohnke, D. and Parthé, E. *Z. Kristallogr. 127* (1968) 164.
11. Parthé, E., Hohnke, D. and Hulliger, F. *Acta Crystallogr. 23* (1967) 832.
12. Rummery, T. E. and Heyding, R. D. *Can. J. Chem. 45* (1967) 131.
13. Barricelli, L. B. *Acta Crystallogr. 11* (1958) 75.
14. Munson, R. A. *Inorg. Chem. 7* (1968) 389.
15. Sövold, L. *Thesis*, University of Oslo, Oslo 1954.
16. Biltz, W., Laar, J., Ehrlich, P. and Meisel, K. *Z. Anorg. Allg. Chem. 233* (1937) 257.
17. Hockings, E. F. and White, J. G. *J. Phys. Chem. 64* (1960) 1042.

Received September 30, 1977.